NANO LETTERS

2008
Vol. 8, No. 10
3109-3113

Secondary Ion Mass Spectrometry of Vapor−Liquid−Solid Grown, Au-Catalyzed, Si Wires

Morgan C. Putnam,*,† Michael A. Filler,‡ Brendan M. Kayes,‡ Michael D. Kelzenberg,‡ Yunbin Guan,§ Nathan S. Lewis,† John M. Eiler,§ and Harry A. Atwater‡

Division of Chemistry and Chemical Engineering, Division of Engineering and Applied Science, and Division of Geological and Planetary Sciences, California Institute of Technology, 1200 East California Boulevard, Pasadena, California 91125

Received April 30, 2008; Revised Manuscript Received July 18, 2008

ABSTRACT

Knowledge of the catalyst concentration within vapor−liquid−solid (VLS) grown semiconductor wires is needed in order to assess potential limits to electrical and optical device performance imposed by the VLS growth mechanism. We report herein the use of secondary ion mass spectrometry to characterize the Au catalyst concentration within individual, VLS-grown, Si wires. For Si wires grown by chemical vapor deposition from $SiCl_4$ at 1000 °C, an upper limit on the bulk Au concentration was observed to be 1.7×10^{16} atoms/cm^3, similar to the thermodynamic equilibrium concentration at the growth temperature. However, a higher concentration of Au was observed on the sidewalls of the wires.

Vapor−liquid−solid (VLS) grown wires are key components of novel solid-state devices and architectures, including photovoltaic cells,[1−5] field-effect transistors,[6,7] light-emitting diodes,[8] photodetectors,[9] and molecular sensors.[10] While these devices appear promising, it is difficult to assess their ultimate potential without greater information concerning the catalyst incorporation in VLS-grown wires. Catalyst atoms within a wire may produce deep-level, carrier recombination centers or cause unintentional doping.[11] For example, Au is the most commonly used catalyst in the VLS growth of Si wires and acts as an effective carrier recombination center in Si, significantly reducing the minority-carrier lifetime.[12]

Efforts to determine Au incorporation in VLS-grown, Si wires have been limited to date. This is due to the submicrometer spatial resolution and better than parts per million chemical sensitivity required to analyze individual wires. In an attempt to meet these stringent requirements, localized electrode atom probe (LEAP) tomography has been used to probe the concentration of Au in 100 nm diameter Si wires grown by chemical vapor deposition (CVD) at 550 °C using SiH_4 as the Si precursor. However, using LEAP tomography, Perea et al. were unable to detect Au in the Si wires and were limited to setting an upper limit on the Au concentration between 5×10^{17} and 1.5×10^{18} atoms/cm^3.[13,14] More recently, high-angle annular dark-field (HAADF) scanning transmission electron microscopy (STEM) has been used to spatially localize single Au atoms within 15 nm diameter Si wires grown by CVD at 450 °C,[14] as well as ∼30 nm diameter Si wires grown by molecular beam epitaxy (MBE) at 500 °C.[15] Again SiH_4 was used as the Si precursor in both reports. HAADF STEM results suggested that for both the CVD and MBE grown Si wires the bulk Au concentration is considerably greater than the thermodynamic equilibrium concentration of Au in Si at the growth temperature. Using a new type of secondary ion mass spectrometry (SIMS) instrument, the Cameca NanoSIMS-50 L, we found the bulk Au concentration to be roughly equal to the thermodynamic equilibrium concentration of Au in Si for Si wires grown by CVD from $SiCl_4$ at 1000 °C and observed an increased Au concentration on the sidewalls of the Si wires.

High-fidelity arrays of well-aligned Si wires, as shown in Figure 1, were grown from patterned Au catalysts on a Si(111) wafer.[16] Single Si wires were analyzed in both the axial and the radial directions. To analyze the wires radially, the wire arrays were sonicated to obtain Si wires suspended in isopropanol. This suspension was then drop-cast onto a Ge(111) wafer to obtain single Si wires lying on their side.

* Corresponding author. E-mail: putnam@caltech.edu.
† Division of Chemistry and Chemical Engineering.
‡ Division of Engineering and Applied Science.
§ Division of Geological and Planetary Sciences.

10.1021/nl801234y CCC: $40.75
Published on Web 09/04/2008

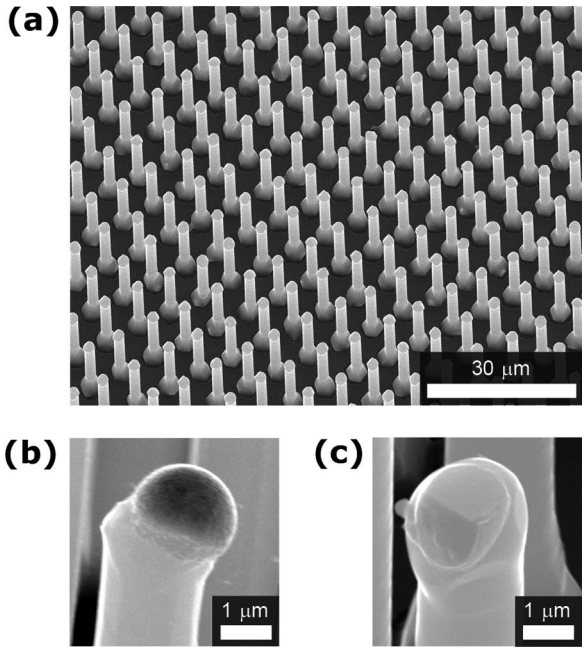

Figure 1. VLS-grown, Au-catalyzed, Si wire arrays were grown on a Si(111) substrate from Au catalyst that had been lithographically patterned and confined by a thermal oxide.[16] Wires were tens of micrometers in length and 2 μm in diameter and were grown in the ⟨111⟩ direction. (a) Tilted SEM image of a Au-etched wire array. (b) Tilted SEM image of a single Si wire tip, prior to Au removal. (c) Tilted SEM image of a single Si wire tip, after Au removal.

Some wire arrays were Au-etched prior to sonication in a manner similar to Woodruff et al.[17] In our procedure, arrays were exposed to Buffer HF Improved (Transene Inc.) for 30 s, rinsed in 18 MΩ cm resistivity deionized (DI) water, immersed in a 9:1 gold etchant TFA (an aqueous solution of I_2 and KI; Transene Inc.):HCl (37%, aq) mixture for 20 min, and rinsed in a 1 M HCl (aq) solution. Arrays were then washed in 18 MΩ cm resistivity DI water and dried in a stream of N_2. After treatment, Au was not detectable on the sidewalls or tips of the wires by electron beam energy-dispersive spectroscopy (EDS). Ellipsometry measurements on a silicon(100) on insulator wafer revealed that our Au etching procedure did not etch Si. For axial analysis, wires were measured in their as-grown vertical orientation. Because of the presence of the catalyst droplet at the wire tip, all axially profiled wires were Au-etched prior to analysis.

A Cameca NanoSIMS-50 L was used for SIMS analysis. In SIMS, a primary ion beam is used to ionize and sputter surface atoms from the sample. The sputtered, ionized surface atoms (secondary ions) are then collected and analyzed in a mass spectrometer. Both radially profiled and axially profiled wires were analyzed at normal incidence with a 16 keV Cs^+ primary ion beam. A 1 μm^2 rastered area, with a centered 0.25 μm^2 gated area, was used to predominantly confine the sputtered area within the wire and to largely confine the collected counts to secondary ions that originated from the center of the sputtered area, as shown in Figure 2a,d and Figure 4a,c. To obtain the Au concentration from the secondary ion count rates, a relative sensitivity factor (RSF) is required; see eq 1.

$$\text{Au concentration} = \text{RSF}\ (\text{atoms/cm}^3) \times \frac{^{197}\text{Au count rate}}{^{30}\text{Si count rate}} \quad (1)$$

The RSF is a function of the impurity and the matrix secondary ion species sampled. To calculate the RSF, a Si(100) wafer (Charles Evans and Associates), with a ^{197}Au implant dose of 1.0×10^{14} atom/cm^2 and a known depth profile, was used as a standard. As there is no reason to suspect otherwise, it is assumed that the Si isotope distribution within the grown wire and the control wafer are the same. A discussion of the beam currents used and the resulting sample sputtering rates can be found in Supporting Information. Additionally, the measured count rates of ^{30}Si, ^{74}Ge, and ^{197}Au secondary ions versus depth for Au-etched Si wires analyzed in both the radial and the axial directions are displayed in Supporting Information, Figure S2.

Figure 2b,c displays the Au concentration profiles for unetched and Au-etched, radially profiled wires. In both cases, the Au concentration was larger near the surface than in the bulk (center) of the wires. By comparing the unetched and the Au-etched wires, a large difference in both the near-surface and the bulk Au concentrations was observed. As the Au removal does not appreciably etch Si, the differences between the two Au concentration profiles are ascribed to a difference in the amount of Au present at the surface of the wires before and after the Au etch.

The observed exponential decay of the near-surface Au concentration profiles for the unetched and Au-etched Si wires can be understood given the nature of the SIMS characterization method. In SIMS, the ion implantation of Cs^+ amorphizes and mixes the surface of the sample over the mean Cs^+ implant depth.[18] As a result of this mixing, a Au layer residing on the sidewalls of the wires would produce an exponential decay in the observed Au concentration profile. This is seen for the Au-etched wires, though a single exponential decay is less obvious for the unetched wires. The perturbation from a single exponential decay for the unetched wires is not yet well-understood but may arise from the more diffuse primary ion beam during analysis of the unetched wires (see Supporting Information).

Given the evidence for the observed near-surface Au concentration arising from Au on the sidewalls of the wires and a mechanism by which Au could be mixed to a greater depth within the wire, it is reasonable to estimate the surface Au concentration by integrating the Au concentration profile for the unetched Si wire over the depth of the near-surface region (Figure 2b). Integrating from 0 to 400 nm yields an estimate for the surface Au concentration on the order of 1 monolayer.

Further examining the observed surface Au concentration, one finds that it is larger at the front surface than at the back surface of the wires. This difference in the surface Au concentration seems unreasonable, given the radial symmetry of the wires. A possible origin of the asymmetry in the surface Au concentration is a decrease in ^{197}Au collection

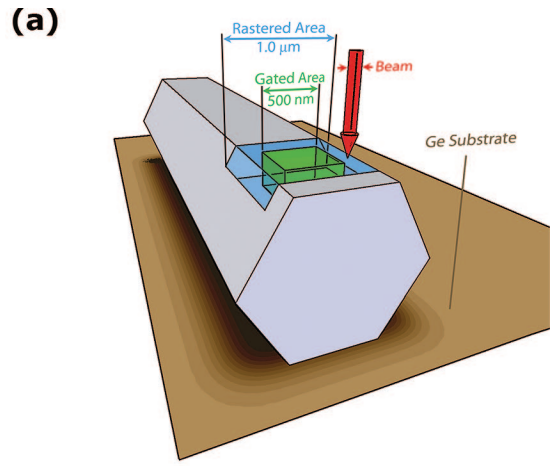

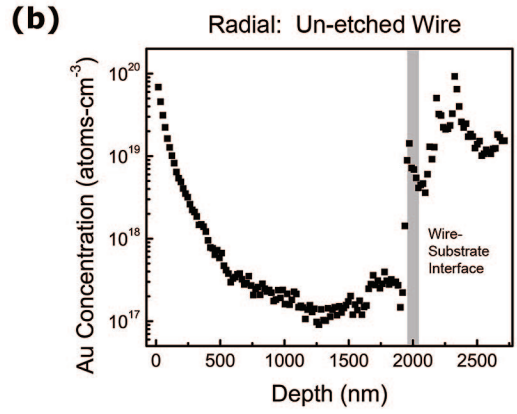

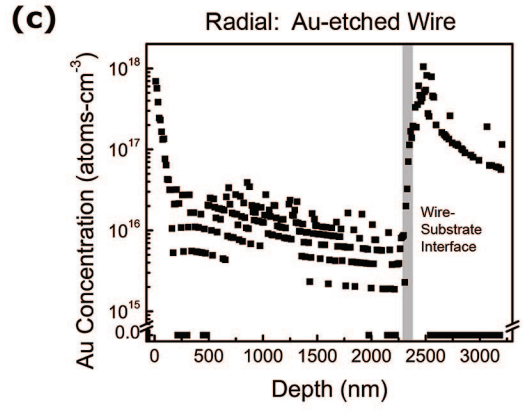

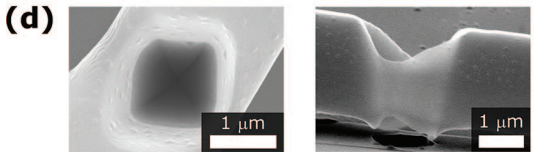

Figure 2. (a) Schematic of the radial-analysis geometry. (b) Radial Au concentration profile of an unetched, VLS-grown, Si wire. (c) Radial Au concentration profile of a Au-etched, VLS-grown, Si wire. The apparent lines in the Au concentration profile, for the Au-etched wire, reflect the fact that the detection limit was approached under our analysis conditions and that integer counts per cycle time period must be obtained. In b and c, the vertical, gray band corresponds to the Si wire/Ge substrate interface, defined as the transition region from 16% to 84% of the maximum count rate for either ^{30}Si or ^{74}Ge. (d) Top-down and tilted SEM images of a radially profiled wire.

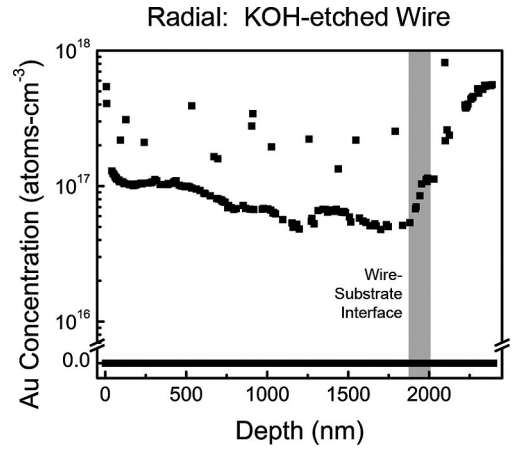

Figure 3. Radial Au concentration profile for a KOH-etched, Au-etched, VLS-grown Si wire. The vertical, gray band corresponds to the Si wire/Ge substrate interface, defined as the transition region from 16% to 84% of the maximum count rate for either ^{28}Si (see *unrastered analysis conditions* in Supporting Information) or ^{74}Ge. Note the observed zero Au concentration values in the Au concentration profile.

efficiency (Figure S2), conceivably because of the large aspect ratio of the sputtered crater when sampling the back surface. It is important to note that the elevated Au concentration observed within the Ge wafer, seen for both wires, is an artifact of the decreased ^{30}Si count rate within the Ge wafer.

Comparing the observed bulk Au concentrations for the unetched and Au-etched Si wires, one notes an order of magnitude higher Au concentration for the unetched Si wire (Figure 2b,c). Since the Au concentration profile for the unetched wire exhibits a nearly constant value ($\sim 2 \times 10^{17}$ atoms/cm^3) between 1000 and 1500 nm, the larger bulk Au concentration observed for this wire is unlikely to be due to Au from the sidewall of the wire that was mixed to a greater depth. Rather, it is likely that a small fraction of secondary ions from outside the rastered area are being collected. Given the high surface Au concentration, collecting only one secondary ion in 200 from outside of the rastered area would produce the observed bulk Au concentration for the unetched wire.

To obtain an estimate for the bulk Au concentration, the observed Au concentration was averaged over the first half of the Au-etched wires (not including the near-surface region), where the effects of the high-aspect ratio sputtered area should be smallest (Figure 2c). For the five, Au-etched, radial profiles, the average Au concentration within the bulk of the wire was $1.7 \pm 0.7 \times 10^{16}$ atoms/cm^3. The internal error of the measurement is estimated to be $<15\%$.[19] Given the high surface Au concentration still present for the Au-etched wires and the potential to collect counts from the sidewalls of the wires, the average bulk Au concentration is best viewed as an upper limit.

With the addition of a KOH etch (10 s Buffered HF Improved followed by 2−3 s in a 50 wt % KOH solution at 55 °C; see Supporting Information) to remove ~20 nm of the surface Si, an increased Au concentration at the surface of the wire was no longer observed, as shown in Figure 3.

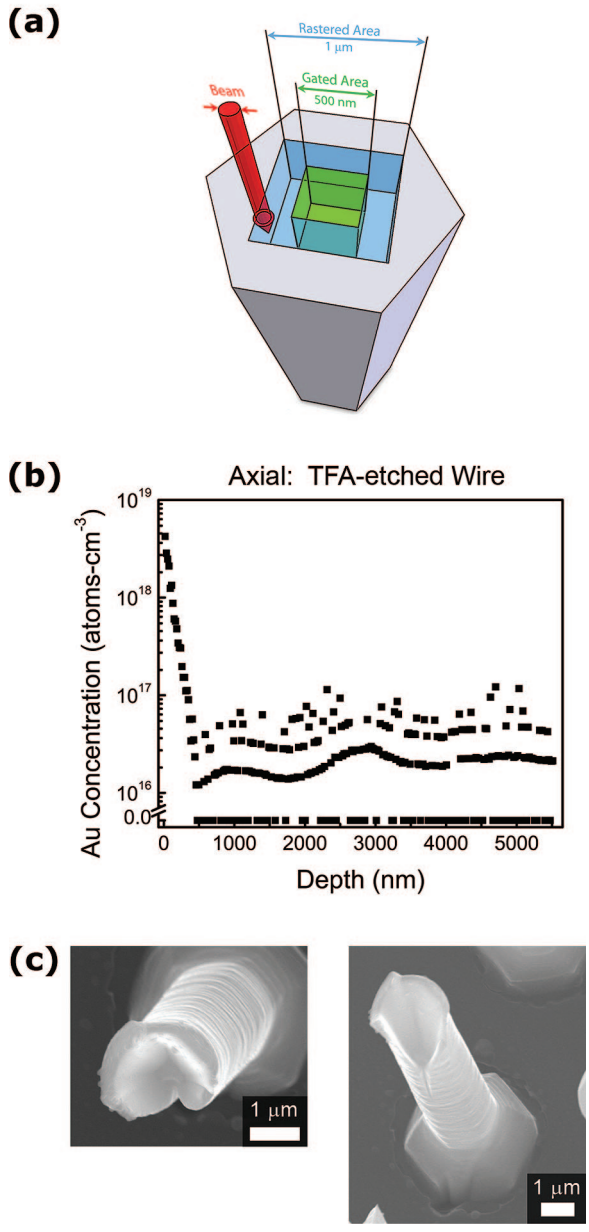

Figure 4. (a) Schematic of the axial-analysis geometry. (b) Axial Au concentration profile of a Au-etched, VLS-grown, Si wire. The apparent lines in the Au concentration profile reflect the fact that the detection limit was approached under our analysis conditions and that integer counts per cycle time period must be obtained. (c) Top-down and tilted SEM images of an axially profiled wire.

The as-measured secondary ion count rates versus depth can be found in Supporting Information, Figure S2c. For the two KOH-etched wires, the average bulk Au concentrations were 1.2×10^{16} atoms/cm^3 and 0.9×10^{16} atoms/cm^3, demonstrating that the bulk Au concentration is on the order of 10^{16} atoms/cm^3. Again, the average was performed over the first half of the wire. The unrastered analysis conditions (see Supporting Information) used to measure the KOH-etched wires resulted in a larger internal error for the bulk Au concentration. Therefore, we believe that the Au-etched data reflect the most conservative upper bound on the bulk Au concentration.

Figure 4 depicts the Au concentration profile observed when a Au-etched, Si wire was axially profiled. For the wire shown, the observed Au concentration decreased exponentially from 6×10^{18} atoms/cm^3 at the surface to an average of 2.4×10^{16} atoms/cm^3 within the bulk of the wire, while a second axially profiled wire exhibited a surface Au concentration of 8×10^{18} atoms/cm^3 and an average bulk Au concentration of 5.0×10^{16} atoms/cm^3. As compared with the Au-etched, radially profiled wires, the observed surface Au concentrations for the Au-etched, axially profiled wires are a factor of 7 larger. This difference is reasonable given that the rapid cooling of the Au−Si alloy at the wire tip produces a Au−Si region that is difficult to etch (images not shown). In contrast, the average bulk Au concentration is expected to be similar for both the axially and the radially profiled wires. While the axially profiled wires exhibited a few-fold higher bulk Au concentration, the sputtering of the wire sidewall that occurred in the axial geometry, shown in Figure 4c, would be capable of producing this difference.

The increased Au concentration on the sidewalls of the wires may result from a Au−Si phase that is present during growth. The existence of a Au−Si phase on the sidewalls of VLS-grown, Au-catalyzed, Si wires during growth has been suggested previously for Si wires grown with Si_2H_6 as the Si precursor,[20] and Au clusters, possibly indicators of the existence of a Au−Si surface phase, have been found on the surface of Si wires grown with SiH_4.[21,22] In our work, for the two unetched wires measured, the integrated amount of Au over the surface region was on the order of 1 monolayer, which would be consistent with the existence of a Au−Si surface phase.[23]

Our observed upper limit on the bulk Au concentration of 1.7×10^{16} atoms/cm^3 is comparable to the 1×10^{16} atoms/cm^3 thermodynamic equilibrium concentration of Au in Si at the growth temperature of 1000 °C.[24] The observed upper limit represents a chemical sensitivity to Au in Si of ~400 ppb. For the VLS growth method, the Au−Si phase diagram should determine the bulk Au concentration within the Si wire provided that the diffusion kinetics are sufficiently rapid to enable the establishment of the thermodynamic equilibrium Au concentration within the wire. Thus, we expect the bulk Au concentration within our 2 μm diameter Si wires to be representative of the bulk Au concentrations for Si wires ranging from tens of nanometers to many micrometers in diameter, as long as the Au−Si phase diagram is similar across the range of diameters and the wires are grown under our growth conditions.

A bulk Au concentration of 1.7×10^{16} atoms/cm^3 in Si is expected to yield a minority-carrier recombination lifetime of 3 ns for both electron and hole minority carriers.[24] In a radial-junction photovoltaic cell, with dopant concentrations of 10^{18} dopants/cm^3 for both n- and p-type regions, a 3 ns minority-carrier recombination lifetime would lead to minority-carrier diffusion lengths of 1 μm for both electrons and holes.[12] These diffusion lengths can be used to guide radial-junction photovoltaic device design, specifically to determine the optimal wire radius.[25] Additionally, these results agree reasonably well with the 2 μm effective hole diffusion length

that has recently been observed by scanning photocurrent microscopy on similar VLS-grown, Au-catalyzed, Si wires with a n-type doping level of 10^{18} atoms/cm^3.[5]

The two key findings of this work are an upper limit on the bulk Au concentration similar to the thermodynamic equilibrium concentration of Au in Si at the growth temperature and an increased Au concentration on the sidewalls of the wires. These results are for Au-catalyzed, Si wires grown by CVD at 1000 °C using $SiCl_4$ as a Si precursor. In contrast, HAADF STEM results indicate a bulk Au concentration much greater than the thermodynamic equilibrium concentration of Au in Si at the growth temperature for Au-catalyzed, Si wires grown by CVD and MBE at temperatures of 450 and 500 °C, respectively, using SiH_4 as a Si precursor. HAADF STEM results also revealed an increased Au concentration near the sidewalls of the wires for the MBE grown wires but not for the CVD grown wires.[14,15] While these differences can not yet be fully explained, it is possible that they are related to changes in the growth temperature, the surface chemistry, and/or the Au−Si phase diagram between the various growth conditions and the wire diameters.

Acknowledgment. The authors thank BP and the Caltech Center for Sustainable Energy Research for support and acknowledge use of facilities of the Center for the Science of Materials, an NSF MRSEC. The authors also thank Jen Dionne for SEM support.

Supporting Information Available: Further experimental details, sputtering volumes, and count rates. This material is available free of charge via the Internet at http://pubs.acs.org.

References

(1) Maiolo, J. R.; Kayes, B. M.; Filler, M. A.; Putnam, M. C.; Kelzenberg, M. D.; Atwater, H. A.; Lewis, N. S. *J. Am. Chem. Soc.* **2007**, *129* (41), 12346–12347.
(2) Goodey, A. P.; Eichfeld, S. M.; Lew, K. K.; Redwing, J. M.; Mallouk, T. E. *J. Am. Chem. Soc.* **2007**, *129*, 12344–12345.
(3) Tian, B. Z.; Zheng, X. L.; Kempa, T. J.; Fang, Y.; Yu, N. F.; Yu, G. H.; Huang, J. L.; Lieber, C. M. *Nature* **2007**, *449* (7164), 885−889.
(4) Tsakalakos, L.; Balch, J.; Fronheiser, J.; Korevaar, B. A.; Sulima, O.; Rand, J. *Appl. Phys. Lett.* **2007**, *91* (23), 233117–3.
(5) Kelzenberg, M. D.; Turner-Evans, D. B.; Kayes, B. M.; Filler, M. A.; Putnam, M. C.; Kelzenberg, M. D.; Lewis, N. S.; Atwater, H. A. *Nano Lett.* **2008**, *8* (2), 710–714.
(6) Cui, Y.; Zhong, Z. H.; Wang, D. L.; Wang, W. U.; Lieber, C. M. *Nano Lett.* **2003**, *3* (2), 149–152.
(7) Bryllert, T.; Wernersson, L. E.; Froberg, L. E.; Samuelson, L. *IEEE Electron Device Lett.* **2006**, *27* (5), 323–325.
(8) Qian, F.; Gradecak, S.; Li, Y.; Wen, C. Y.; Lieber, C. M. *Nano Lett.* **2005**, *5* (11), 2287–2291.
(9) Gu, Y.; Kwak, E. S.; Lensch, J. L.; Allen, J. E.; Odom, T. W.; Lauhon, L. J. *Appl. Phys. Lett.* **2005**, *87* (4), 043111–3.
(10) Wan, Q.; Li, Q. H.; Chen, Y. J.; Wang, T. H.; He, X. L.; Li, J. P.; Lin, C. L. *Appl. Phys. Lett.* **2004**, *84* (18), 3654–3656.
(11) Sze, S. M. *Physics of Semiconductor Devices*; Wiley-Interscience: New York, 1981.
(12) Pierret, R. F. *Advanced Semiconductor Fundamentals*; Prentice Hall: Upper Saddle River, NJ, 2003; Vol. VI.
(13) Perea, D. E.; Lensch, J. L.; May, S. J.; Wessels, B. W.; Lauhon, L. J. *Appl. Phys. A* **2006**, *85* (3), 271–275.
(14) Allen, J. E.; Hemesath, E. R.; Perea, D. E.; Lensch-Falk, J. L.; Li, Z. Y.; Yin, F.; Gass, M. H.; Wang, P.; Bleloch, A. L.; Palmer, R. E.; Lauhon, L. J. *Nat. Nanotechol.* **2008**, *3*, 168–173.
(15) Oh, S. H.; Benthem, K.; Molina, S. I.; Borisevich, A. Y.; Luo, W.; Werner, P.; Zakharov, N. D.; Kumar, D.; Pantelides, S. T.; Pennycook, S. J. *Nano Lett.* **2008**, *8* (4), 1016–1019.
(16) Kayes, B. M.; Filler, M. A.; Putnam, M. C.; Kelzenberg, M. D.; Lewis, N. S.; Atwater, H. A. *Appl. Phys. Lett.* **2007**, *91* (10), 103110–3.
(17) Woodruff, J. H.; Ratchford, J. B.; Goldthorpe, I. A.; McIntyre, P. C.; Chidsey, C. E. D. *Nano Lett.* **2007**, *7* (6), 1637–1642.
(18) Wilson, R. G.; Stevie, F. A.; Magee, C. W. *Secondary Ion Mass Spectroscopy*; John Wiley and Sons: New York, 1989.
(19) The total internal error is found by taking the root of the sum of the squares of the internal errors. The two dominant internal errors arise from the counting statistics for the ^{197}Au secondary ions and the measurement of the average sputtered depth on the standard.
(20) Hannon, J. B.; Kodambaka, S.; Ross, F. M.; Tromp, R. M. *Nature* **2006**, *440* (7080), 69–71.
(21) Dhalluin, F.; Desre, P. J.; Hertog, M. I.; Rouviere, J. L.; Ferret, P.; Gentile, P.; Baron, T. *J. Appl. Phys.* **2007**, *102* (9), 094906–5.
(22) Hertog, M. I.; Rouviere, J. L.; Dhalluin, F.; Desre, P. J.; Gentile, P.; Ferret, P.; Oehler, F.; Baron, T. *Nano Lett.* **2008**, *8* (5), 1544–1550.
(23) Slezak, J.; Ondrejcek, M.; Chvoj, Z.; Chab, V.; Conrad, H.; Heun, S.; Schmidt, T.; Ressel, B.; Prince, K. C. *Phys. Rev. B* **2000**, *61* (23), 16121–16128.
(24) Bullis, W. M. *Solid-State Electron.* **1966**, *9* (2), 143–168.
(25) Kayes, B. M.; Atwater, H. A.; Lewis, N. S. *J. Appl. Phys.* **2005**, *97* (11), 114302–11.

NL801234Y